between ^{13}C depletion and ambient pCO_2 values (*39–41*). However, Δ_C values for the Permo-Carboniferous are larger than values immediately before and after this time span, a feature difficult to explain in terms of greatly increased pCO_2. Indeed, Permo-Carboniferous CO_2 concentration is likely to have been decidedly lower than during the preceding and succeeding periods (*32*). The paradox might be resolved if the pO_2 of the Permo-Carboniferous reached 35%, a value indicated by modeling, because a greater measured Δ_C at this time could be explained without relying entirely on the burial of anomalously ^{13}C-depleted OM (*33*). Plant growth experiments demonstrate that plants can grow in atmospheres of up to 40% O_2 (*42*) with the balance between vegetative and reproductive growth remaining unaffected, indicating the possibility of maintaining viable populations under such conditions. Furthermore, a value of 35% O_2 (with $pCO_2 = 300$ ppm) is compatible with continued biogeochemical cycling of carbon by terrestrial ecosystems (*43*). Other physiological studies suggest that elevated pO_2 during the Permo-Carboniferous may help explain patterns in evolution. Flight metabolism in arthropods is enhanced at elevated O_2 concentrations (*44*), and the sudden rise and subsequent fall of insect gigantism documented from the fossil record by, for example, giant dragonflies with wingspans of 70 cm is coincident with the Permo-Carboniferous maximum in pO_2 (*45, 46*). Other patterns have been linked to elevated O_2, such as changes in organisms with diffusion-mediated respiration and the invasion of the land by vertebrates (*45, 46*).

References and Notes

1. L. V. Berkner and L. C. Marshall, *J. Atmos. Sci.* **22**, 225 (1965).
2. P. E. Cloud, *Paleobiology* **2**, 351 (1976).
3. J. C. G. Walker, *Evolution of the Atmosphere* (Macmillan, New York, 1977).
4. H. D. Holland, *The Chemical Evolution of the Atmosphere and Oceans* (Princeton Univ. Press, Princeton, NJ, 1984).
5. D. J. Des Marais, H. Strauss, R. E. Summons, J. M. Hayes, *Nature* **359**, 605 (1992).
6. W. G. Chaloner, *J. Geol. Soc.* **146**, 171 (1989).
7. A. Watson, J. E. Lovelock, L. Margulis, *Biosystems* **10**, 293 (1978); J. M. Robinson, *Palaeogeogr. Palaeoclimatol. Palaeoecol.* **75**, 223 (1989). Watson *et al*. do not allow for O_2 variations to exceed 25%, whereas Robinson states that this value is not well defined and that the maximum O_2 concentration could be considerably higher. For this study, a maximum concentration of 40% was used.
8. H. D. Holland, *The Chemistry of the Atmosphere and Oceans* (Wiley-Interscience, New York, 1978).
9. R. M. Garrels and A. Lerman, *Am. J. Sci.* **284**, 989 (1984).
10. T. M. Lenton, thesis, Univ. of East Anglia, Norwich, UK (1998).
11. H. D. Holland, *Eos* **75**, OS96 (1994).
12. P. Van Cappellen and E. D. Ingall, *Science* **271**, 493 (1997).
13. A. S. Colman, F. T. Mackenzie, H. D. Holland, *Science* **275**, 406 (1998).
14. R. A. Berner and S. T. Petsch, *Science* **282**, 1426 (1998).
15. R. A. Berner and D. E. Canfield, *Am. J. Sci.* **289**, 333 (1989).
16. R. A. Berner, *Am. J. Sci.* **287**, 177 (1987).
17. G. D. Farquhar *et al*., *Aust. J. Plant Physiol.* **9**, 121 (1982).
18. W. M. Sackett, B. J. Eadie, M. L. Bender, A. W. H. Be, *Science* **148**, 235 (1965).
19. D. E. Canfield and A. Teske, *Science* **382**, 127 (1996).
20. L. M. Francois and J. C. Gerard, *Geochim. Cosmochim. Acta* **50**, 2289 (1987).
21. L. R. Kump and R. M. Garrels, *Am. J. Sci.* **286**, 336 (1986).
22. S. T. Petsch and R. A. Berner, *Am. J. Sci.* **298**, 246 (1998).
23. A. C. Lasaga, *Am. J. Sci.* **289**, 411 (1989).
24. D. J. Beerling and F. I. Woodward, in *Stable isotopes. Integration of Biological, Ecological and Geochemical Processes*, H. Griffiths, Ed. (BIOS Publishers, Oxford, 1998), pp. 347–361.
25. J. S. Gillon and H. Griffiths, *Plant Cell Environ.* **20**, 1217 (1997).
26. *R. repens* and *M. communis* seeds were germinated and cultivated on the same medium at 22°C and 70% relative humidity with irradiance of 250 μmol m^{-2} s^{-1}. After 6 weeks (*R. repens*) or 12 weeks (*M. communis*) of growth, seedlings were transferred to controlled growth chambers [design, replication, and environmental regulation detail are given in (*43*)] with either 21 or 35% O_2 and a constant (monitored and controlled) concentration of 330 ppm CO_2. Growth chamber relative humidity was 60 ± 10% and irradiance was 250 μmol m^{-2} s^{-1} under a diurnal cycle of 14 hours of light (at 21°C) and 10 hours of darkness (at 18°C). Plants were watered daily with 40 ml of dilute Rorison's solution.
27. Mature whole leaves were harvested, dried (for 4 days at 30°C), and powdered. (Studies have shown that differences between leaves from different plants or growth conditions are mirrored by the same differences in stems.) Samples were combusted to CO_2 and analyzed in triplicate at the Biomedical Mass Spectrometry Unit, University of Newcastle, UK. Gas samples exiting the growth chambers were collected and CO_2 was isolated and processed as above.
28. E. A. Laws, B. N. Popp, R. R. Bidigare, M. C. Kennicutt, S. A. Macko, *Geochim. Cosmochim. Acta* **59**, 1131 (1995).
29. B. N. Popp *et al*., *Geochim. Cosmochim. Acta* **62**, 69 (1998).
30. E. A. Laws, R. R. Bidigare, B. N. Popp, *Linmol. Oceanogr.* **42**, 1552 (1997).
31. From the relation between $[O_2]_{aq}/[CO_2]_{aq}$ and Obs.-Pred. shown in Table 2, along with the solubility of O_2 and CO_2 in seawater as a function of temperature, we calculated the values of $\Delta(\Delta_C)$ that were appropriate for different pO_2 values and a fixed value of atmospheric CO_2 (330 ppm) and temperature (25°C).
32. R. A. Berner, *Science* **276**, 544 (1997).
33. J. M. Hayes, H. Strauss, A. J. Kaufman, *Chem. Geol.* **161**, 103 (1999).
34. The relation between ^{13}C discrimination and pO_2 is modeled by first calculating the changes in the ratio of intracellular to ambient CO_2 concentration from a coupled photosynthesis model [G. D. Farquhar and S. C. Wong, *Aust. J. Plant Physiol.* **11**, 191 (1984)] and using this ratio to predict ^{13}C discrimination with the well-validated isotope fractionation model given in (*17*).
35. B. N. Popp, T. F. Anderson, P. A. Sandberg, *Geol. Soc. Am. Bull.* **97**, 1262 (1986).
36. J. Veizer *et al*., *Chem. Geol.* **161**, 59 (1999).
37. A. Paytan, M. Kastner, D. Campbell, M. H. Thiemens, *Science* **282**, 1459 (1998).
38. T. B. Lindh, thesis, Univ. of Miami, Miami, FL (1984).
39. B. N. Popp, R. Takigiku, J. M. Hayes, J. Wm. Louda, E. W. Baker, *Am. J. Sci.* **289**, 436 (1989).
40. K. H. Freeman and J. M. Hayes, *Global Biogeochem. Cycles* **6**, 185 (1992).
41. M. Pagani, M. A. Arthur, K. H. Freeman, *Paleoceanography* **14**, 273 (1999).
42. B. Quebedeaux and R. W. F. Hardy, *Plant Physiol.* **55**, 102 (1975).
43. D. J. Beerling *et al*., *Philos. Trans. R. Soc. London Ser. B* **353**, 131 (1998).
44. J. F. Harrison and J. R. B. Leighton, *J. Exp. Biol.* **201**, 1739 (1998).
45. J. B. Graham, R. Dudley, N. M. Aguilar, C. Gans, *Nature* **375**, 117 (1995).
46. R. Dudley, *J. Exp. Biol.* **201**, 1043 (1998).

47. R.A.B. was supported by Department of Energy grant DE-FGO2-95ER14522 and NSF grant EAR-9804781. J.A.L. and D.J.B. gratefully acknowledge funding through a University of Sheffield Alfred Denny research studentship and a Royal Society University Research Fellowship, respectively. Study of carbon isotopic fractionation in marine microalgae at the University of Hawaii has been supported by NSF grants OCE-9301204 and OCE-9633091 to B.N.P., R. R. Bidigare, E.A.L., and S. G. Wakeham and by grant OCE-9521332 to B.N.P. and E.A.L. We thank G. Farquhar, A. Colman, F. Mackenzie, and S. Smith for helpful comments. This is SOEST contribution number 5013.

30 September 1999; accepted 2 February 2000

Natural $NaAlSi_3O_8$-Hollandite in the Shocked Sixiangkou Meteorite

Philippe Gillet,[1]* Ming Chen,[2,3] Leonid Dubrovinsky,[4] Ahmed El Goresy[2]

The hollandite high-pressure polymorph of plagioclase has been identified in shock-induced melt veins of the Sixiangkou L6 chondrite. It is intimately intergrown with feldspathic glass within grains previously thought to be "maskelynite." The crystallographic nature of the mineral was established by laser micro-Raman spectroscopy and x-ray diffraction. The mineral is tetragonal with the unit cell parameters $a = 9.263 \pm 0.003$ angstroms and $c = 2.706 \pm 0.003$ angstroms. Its occurrence with the liquidus pair majorite-pyrope solid solution plus magnesiowüstite sets constraints on the peak pressures that prevailed in the shock-induced melt veins. The absence of a calcium ferrite–structured phase sets an upper bound for the crystallization of the hollandite polymorph near 23 gigapascals.

Alkali feldspars in the system $KAlSi_3O_8$-$NaAlSi_3O_8$ are abundant minerals in Earth's crust. Their behavior under moderate pressure and temperature (*P-T*) conditions is well-known. For instance, the albite to jadeite + quartz transition is a well-calibrated

metamorphic reaction used to infer the *P-T* conditions of feldspar-rich blueschist and eclogitic rocks (*1*). The behavior of feldspars at higher pressures (>3 GPa) and temperatures (>1000 K) is also of interest because these phases might host K and Na, as well as other important trace elements like Sr or Rb, in Earth's mantle. As shown by recent seismic tomographic images, the continental and oceanic crust can be subducted in the upper and lower mantle (*2*). Feldspars or their high-pressure polymorphs, if stable under the relevant *P-T* conditions, can therefore act as potential carrier of Na, Al, K, and trace elements, from Earth's surface down into the deep mantle.

The behavior of alkali feldspars at *P-T* conditions of Earth's mantle has been experimentally studied. It has been shown that $KAlSi_3O_8$ and $NaAlSi_3O_8$ transform at 1300 K into a denser phase with the hollandite structure at 12 GPa and 21 to 24 GPa, respectively (*3, 4*). Several other silicates with the hollandite structure have also been synthesized (*5–7*). Experiments performed in the $KAlSi_3O_8$-$NaAlSi_3O_8$ system at pressures between 5 and 23 GPa and at temperatures ranging from 1000 to 1500 K have provided more complex results (*8*). $KAlSi_3O_8$-hollandite is stable for pressures that are >10 GPa. $NaAlSi_3O_8$-albite transforms to jadeite + stishovite and then, at 23 GPa, transforms to $NaAlSiO_4$ (calcium ferrite structure) + stishovite; $NaAlSi_3O_8$-hollandite seems to be unstable at such conditions, and it has been concluded that it should be stable at much higher temperatures (*8*). It has also been shown that, at 1300 K, the $NaAlSi_3O_8$ component gradually dissolves into the hollandite structure with increasing pressure and that the maximum solubility is 40 mole percent (mol%) at 23 GPa. The high-pressure polymorphs of feldspars have never been observed in natural terrestrial and extraterrestrial samples. Here, we show the existence of such minerals in the veins of the heavily shocked Sixiangkou meteorite (L6 chondrite) (*9*). Several phases that are thought to occur in the mantle have been synthesized in laboratory experiments and have been observed in shocked chondrites (*10–12*).

The Sixiangkou meteorite contains black veins 0.1 to 2 mm in width formed by shock melting and in which two distinct high-pressure assemblages have been described: (i) majorite-pyrope$_{ss}$ plus magnesiowüstite (ss, solid solution) that crystallized at high pressures and temperatures from a shock-induced silicate melt having the bulk composition of the unmelted parts of the meteorite and (ii) ringwoodite plus low-calcium majorite produced by solid state transformation of olivine and low-calcium pyroxene (*9*). Beside these mineral assemblages, the veins of the meteorite contains, as in most shocked meteorites, zones of feldspathic composition (Fig. 1 and Tables 1 and 2). These zones, often called maskelynite, have been interpreted as diaplectic glasses formed by shock-induced solid state amorphization (*13–15*). More recently they have also been interpreted as quenched products from a high-temperature and high-pressure liquid associated with the residual heat from the shock event (*16*). The maskelynites often display radiating cracks starting from their surfaces and fracturing the neighboring ringwoodite. These cracks are usually filled with material of the same plagioclase composition (Fig. 1). This indicates that the fractured plagioclase was once molten and the melt was injected into these cracks at high pressure.

We characterized the feldspathic material in the Sixiangkou meteorite using electron microprobe, Raman spectroscopy, and x-ray diffraction. The last two techniques permit an unambiguous determination of the glassy versus crystalline nature of the samples. They also have the advantage of being less destructive than transmission electron microscopy, which can lead, in the case of metastable high-pressure phases, to amorphization under the electron beam (*11*). At low magnification, the maskelynites appear homogeneous with typical plagioclase composition, similar from grain to grain and close to those of the feldspars observed in the untransformed parts of the meteorite as already observed in many other shocked meteorites (Tables 1 and 2). Backscattered electron (BSE) images of the grains at high magnification using a field-emission scanning electron microscope

[1]Laboratoire de Sciences de la Terre, Ecole Normale Supérieure de Lyon et Université Claude Bernard Lyon I (UMR CNRS 5570), 46, allée d'Italie, 69364 Lyon Cedex, France. [2]Max-Planck-Institut für Chemie, Joachim-Becher-Weg 27, D-55128 Mainz, Germany. [3]Guangzhou Institute of Geochemistry, AC, Guangzhou, China. [4]Theoretical Geochemistry Program, Institute of Earth Sciences, Uppsala University, S-75236 Uppsala, Sweden.

*To whom correspondence should be addressed. E-mail: pgillet@ens-lyon.fr

Table 1. Chemical composition of plagioclase (Pl) and maskelynite (Ms) in Sixiangkou and other L6 chondrites (values in weight %).

Oxide	Sixianghou		Tenham		Peace River		Dar Al Gani 355	
	Pl	Ms	Pl	Ms	Pl	Ms	Pl	Ms
SiO_2	65.01	65.21	66.50	67.62	65.01	65.84	65.37	66.55
Al_2O_3	21.00	21.65	22.68	22.99	23.35	21.65	21.08	22.35
K_2O	0.98	1.46	0.87	1.08	0.69	2.37	0.32	1.64
Na_2O	9.61	9.24	7.29	5.62	8.37	6.56	9.97	8.14
CaO	2.08	2.20	2.13	2.01	2.29	2.19	2.11	1.69
MgO	0.03	0.34	0.06	0.02	0.00	0.02	0.07	0.08
FeO	0.29	0.75	0.54	0.48	0.38	0.52	0.51	0.42
Total	99.00	99.85	100.07	99.84	100.09	99.15	99.43	100.87

Table 2. Elements [number of cations (O = 8)] of plagioclase and maskelynite in Sixiangkou and other L6 chondrites.

Element	Sixianghou		Tenham		Peace River		Dar Al Gani 355	
	Pl	Ms	Pl	Ms	Pl	Ms	Pl	Ms
Si	2.89	2.89	2.89	2.93	2.85	2.91	2.89	2.90
Al	1.10	1.08	1.17	1.17	1.20	1.13	1.10	1.14
K	0.06	0.08	0.05	0.06	0.04	0.13	0.02	0.09
Na	0.83	0.79	0.61	0.47	0.71	0.56	0.85	0.69
Ca	0.09	0.10	0.13	0.09	0.11	0.11	0.08	0.08
Mg	0.00	0.02	0.06	0.02	0.00	0.02	0.07	0.08
Fe	0.29	0.03	0.02	0.02	0.01	0.02	0.02	0.01
Total	4.99	4.99	4.87	4.74	4.92	4.86	4.96	4.91

Fig. 1. Photograph of a maskelynite in the Sixiangkou meteorite obtained with a field emission SEM in BSE mode. Scale bar is 10 μm. Maskelynite is surrounded by ringwoodite crystals (rg) and by majorite-pyrope$_{ss}$ + magnesiowüstite (mw + mj). The arrows indicate fractures filled with material of the same composition as maskelynite.

(SEM) revealed a fine-grained network of bright and dark lamellae in the submicrometer range. The composition is that of an oligoclase ($Ab_{80}An_{12}Or_8$), however with higher K_2O content than in the plagioclase of the unmelted matrix. The Raman spectra of the feldspathic material is not characteristic of a fully glassy phase (*17*) (Fig. 2). The spectra are similar in the numerous grains examined so far. They consist of the superposition of large broad peaks characteristic of silicate glasses and sharp peaks characteristic of a crystalline phase. The broad peaks are similar those of $NaAlSi_3O_8$ glass, with a broad intense peak at 490 to 500 cm^{-1}, a shoulder at ~580 cm^{-1}, and a less intense broad peak near 1100 cm^{-1} (*18*). The well-defined peaks do not correspond to any known feldspar polymorph of albitic composition. The Raman spectra can be compared to those of K-rich feldspars experimentally transformed at 22 GPa within the stability field of $KAlSi_3O_8$-hollandite (*19*) (Fig. 2). All of the sharp peaks observed on the Raman spectra of the Sixiangkou maskelynite correspond within a few wave numbers to those of $KAlSi_3O_8$-hollandite. The intense peak at 764 cm^{-1} can be assigned to Si-O stretching vibrations in the SiO_6 octahedra by comparison with a similar intense peak observed in SiO_2-stishovite (*19*). The Raman data represent the suggestion that hollandite of feldspathic composition in the joint system $KAlSi_3O_8$-$NaAlSi_3O_8$-$CaAl_2Si_2O_8$ can occur in natural samples. Most of the observed glass + hollandite intergrowths are surrounded by ringwoodite grains or the liquidus pair majorite-pyrope$_{ss}$ + magnesiowüstite, but in some rare cases, jadeitic pyroxenes have also been found.

To confirm the presence of hollandite in the Sixiangkou meteorite, a 300-μm disk containing a single grain of irregular shape with maximum dimension of ~60 μm, showing the typical Raman spectrum (Fig. 2), was drilled from a petrographic thin section and studied with x-ray microdiffraction (*20*). The diffraction pattern (Fig. 3 and Table 3) consists of a number of reflections of majorite and a second phase. All 15 diffraction lines of the integrated diffraction pattern, which do not correspond to the majorite crystals adjacent to the grain, can be unambiguously indexed in terms of tetragonal hollandite structure with the lattice parameters a = 9.263(3) Å and c = 2.706(3) Å. The corresponding density is 3.80. The lattice parameters are slightly lower than values reported for pure $KAlSi_3O_8$-hollandite (a = 9.324 Å and c = 2.722 Å) (*21*), probably due to additional amounts of Na and Ca in the structure.

From the previous observations, it is possible to propose constraints on the formation and destabilization of $NaAlSi_3O_8$-hollandite during the shock event. Hollandite results either from the solid state transformation of feldspars similar to those present in the untransformed parts of the meteorite or from the crystallization at high pressures of molten feldspars. The difference in K content between hollandite and untransformed feldspars could be the signature of melting of the feldspars and the addition of K that evaporated from the melt vein during the shock. The

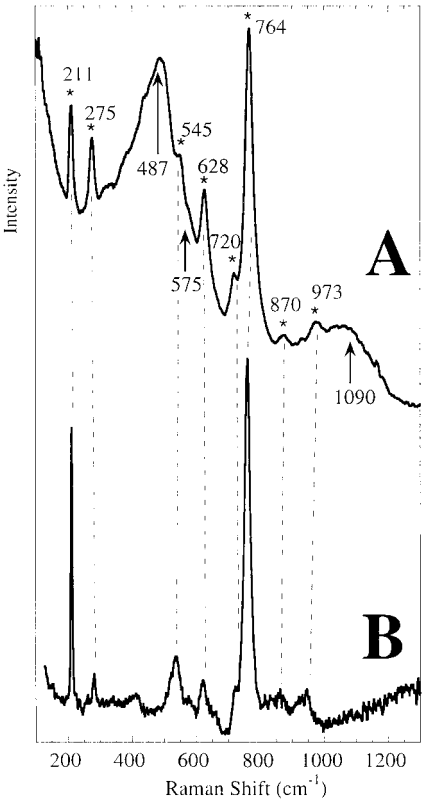

Fig. 2. (**A**) Typical Raman spectrum of the Sixiangkou maskelynites. The broad peaks (arrows) are close to those of $NaAlSi_3O_8$ glass. The sharp peaks (asterisks) belong to hollandite. (**B**) Raman spectrum of $KAlSi_3O_8$-hollandite synthesized at 22 GPa and 1500 K. The sharp peaks of the spectrum in (A) correspond within a few wave numbers to those of $KAlSi_3O_8$-hollandite.

Table 3. Indexed peaks of the x-ray diffraction pattern of the natural high-pressure polymorph of oligoclase with the hollandite structure in the shocked Sixiangkou L6 chondrite. The corresponding spectrum is given in Fig. 3. The cell parameters of tetragonal hollandite of oligoclase composition [a = 9.263(3) Å and c = 2.706(3) Å] compare well with those obtained by Liu (*4*) for the pure $NaAlSi_3O_8$-hollandite [a = 9.30(3) Å and c = 2.73(1) Å] and are close to those of $KAlSi_3O_8$-hollandite reported by Yagi *et al.* (*8*) and Zhang *et al.* (*21*). d_{obs}, observed d spacing; d_{calc}, d spacing calculated with the tetragonal structure and the measured a and b cell parameters. The density is 3.80.

hkl	d_{obs} (Å)	d_{calc} (Å)	$d_{obs} - d_{calc}$ (Å)
110	6.5461	6.5502	−0.0041
200	4.6334	4.6317	0.0017
220	3.2763	3.2751	0.0012
130	2.9314	2.9293	−0.0020
400	2.3173	2.3159	0.0014
211	2.2646	2.2655	−0.0009
240	2.0724	2.0714	0.0010
310	2.0315	2.0351	−0.0034
321	1.8664	1.8632	0.0032
510	1.8162	1.8167	−0.0005
411	1.7372	1.7286	0.0086
600	1.5425	1.5439	−0.0014
251	1.4502	1.4517	−0.0015
002	1.3509	1.3530	−0.0021

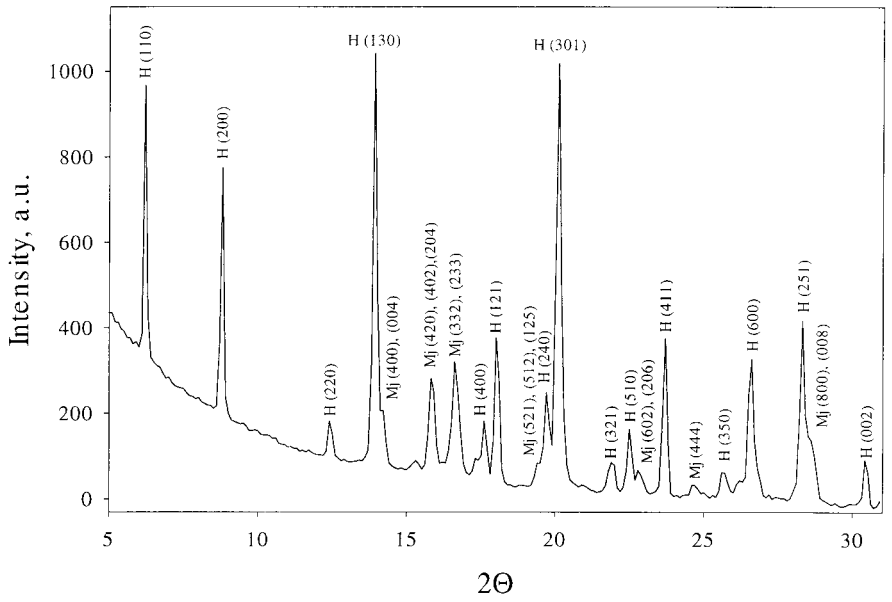

Fig. 3. Diffraction pattern obtained on a maskelynite of the Sixiangkou meteorite. Fifteen diffraction lines (H) are indexed in the hollandite structure (see Table 3). The remaining peaks (Mj) belong to the majorite-pyrope$_{ss}$ grains surrounding the maskelynite.

chemical analysis and the Raman data show that the hollandite crystals are interwoven with glasses of similar composition. In particular, no zone of silica or jadeitic compositions can be distinguished within the grains. The glass can thus either be interpreted as a back-transformation product of hollandite or as a residual liquid quenched during the post-shock pressure and temperature release. The rare occurrence of jadeitic pyroxenes at the rim of some hollandite + glass zones can represent the subsequent transformation (or back transformation) of hollandite into jadeite + SiO_2. However, we have not yet observed zones of SiO_2 composition near the jadeitic grains.

The present study confirms the conclusion of Liu (*4*) that compositions close to the $NaAlSi_3O_8$ end-member system can adopt the hollandite structure. The natural occurrence of hollandite with 8 mol% of $KAlSi_3O_8$ contradicts the work of Yagi *et al.* (*8*), who concluded that the maximum solubility of the $NaAlSi_3O_8$ component in the $NaAlSi_3O_8$-$KAlSi_3O_8$-hollandite solid solution is limited to 40 mol%. Because the temperature conditions during the shock event in the Sixiangkou meteorite are higher than the temperature range experimentally explored by these authors, the present observations indicate that this solubility is temperature dependent.

The occurrence of the liquidus pair majorite-pyrope$_{ss}$ + magnesiowüstite constrains their crystallization at pressures between 21 and 25 GPa and at temperatures between 2273 and 2373 K (*22*). The density of the phases with bulk $NaAlSi_3O_8$ composition increases in the following order: albite < $NaAlSi_2O_6$ (jadeite) + $2SiO_2$ (quartz, coesite, or stishovite) < hollandite < $NaAlSiO_4$ (calcium ferrite) + SiO_2 (stishovite) (*4, 8*). The discovery of hollandite close to the $NaAlSi_3O_8$ end-member puts additional constraints on the shock *P-T* conditions of the Sixiangkou meteorite. The absence of the assemblage $NaAlSiO_4$ (calcium ferrite structure) + $2SiO_2$-stishovite sets the upper pressure bound at 23 GPa (*4, 8*). These data suggest that the formation of the high-pressure assemblages in the shock-induced melt veins in the Sixiangkou meteorite took place at lower pressures but at higher temperatures than previously estimated for shock-induced melt veins in chondritic meteorites (*13, 14*).

References and Notes

1. T. J. B. Holland, *Am. Mineral.* **65**, 129 (1980).
2. R. Van der Hilst, *Nature* **374**, 154 (1995).
3. Hollandite-type compounds possess the general chemical formula $A_xB_8O_{16}$, where A represents large mono- or divalent cations with $x \leq 2$ and B represents small two- to five-valent cations. A. E. Ringwood *et al.* [*Acta Crystallogr.* **23**, 1093 (1967)] transformed sanidine $KAlSi_3O_8$ into the hollandite structure with Al and Si occupying octahedral sites. It was the second silicate, after SiO_2-stishovite, to display sixfold coordination of Si. All of the compounds with the hollandite structure have tetragonal symmetry.
4. $NaAlSi_3O_8$-hollandite was first synthesized by L. Liu [*Earth Planet. Sci. Lett.* **37**, 438 (1978)].
5. R. T. Downs, R. M. Hazen, L. W. Finger, *Am. Mineral.* **80**, 937 (1995).
6. M. Madon, J. Castex, J. Peyronneau, *Nature* **342**, 422 (1989).
7. A. F. Reid and A. E. Ringwood, *J. Solid State Chem.* **1**, 6 (1969).
8. A. Yagi, T. Suzuki, M. Akaogi, *Phys. Chem. Miner.* **21**, 12 (1994).
9. M. Chen, T. G. Sharp, A. El Goresy, B. Wopenka, X. Xie, *Science* **271**, 1570 (1996). These authors have provided a description of the meteorite and its mineralogy.
10. The high-pressure polymorphs of olivine α-$(Mg,Fe)_2SiO_4$ and the $(Mg,Fe)SiO_3$-majorite phases have been reported in many meteorites [see A. J. Brearley and R. H. Jones, in *Planetary Materials*, vol. 36 of *Reviews in Mineralogy*, J. J. Papike, Ed. (Mineralogical Society of America, Washington, DC, 1998), pp. 1–398].
11. $(Mg,Fe)SiO_3$-ilmenite has been discovered in the Tenham meteorite [T. G. Sharp, C. M. Lingemann, C. Dupas, D. Stöffler, *Science* **277**, 352 (1997)].
12. $(Mg,Fe)SiO_3$-perovskite has been discovered in the Tenham meteorite [N. Tomioka and K. Fujino, *Science* **277**, 1084 (1997)].
13. D. Stöffler, A. Bischoff, V. Buchwald, A. E. Rubin, in *Meteorites and the Early Solar System*, J. F. Kerridge and M. S. Matthews, Eds. (Univ. of Arizona Press, Tucson, 1988), pp. 165–202.
14. D. Stöffler, K. Keil, E. R. D. Scott, *Geochim. Cosmochim. Acta* **55**, 3845 (1991).
15. P. Richet and P. Gillet, *Eur. J. Mineral.* **9**, 907 (1997).
16. A. El Goresy, B. Wopenka, M. Chen, G. Kurat, *Meteoritics* **32**, A38, (1997)
17. Raman spectra were recorded with a Dilor XY spectrometer equipped with confocal optics and a nitrogen-cooled charge-coupled device (CCD) detector. A microscope was used to focus the excitation laser beam (488- and 514-nm lines of a Spectra-Physics Ar^+ laser) to a 2-μm spot and to collect the Raman signal in the backscattered direction. Accumulations lasting from 120 to 300 s were made. The laser power was 2 to 50 mW to avoid deterioration of the sample.
18. F. A. Seifert, B. O. Mysen, D. Virgo, *Am. Mineral.* **67**, 696 (1982).
19. Pieces of the M'bale L6 chondrite have been pressurized to 22 GPa and 1500 K in a multianvil press [high-pressure facility at the Bayerisches Geoinstitut (Bayreuth, Germany)] in the stability field of $KAlSi_3O_8$-hollandite. Nearly pure $KAlSi_3O_8$-orthoclase of the starting material has been transformed to a new phase, presumably $KAlSi_3O_8$-hollandite. The Raman spectrum of this phase (Fig. 2) is different from that of orthoclase, which is characterized by strong bands near 500 and 950 cm^{-1}, characteristic of stretching vibrations of SiO_4 tetrahedra. The Raman spectra of $KAlSi_3O_8$- and $NaAlSi_3O_8$-hollandite resemble that of stishovite [R. J. Hemley, H. K. Mao, E. C. T. Chao, *Phys. Chem. Miner.* **13**, 285 (1986)]. The small difference in the Raman frequencies between $(Ab_{80}An_{12}Or_8)$- and $KAlSi_3O_8$-hollandite is accounted for by the small difference in cell parameters (see Table 3).
20. The x-ray facility used in this study includes a rotating anode generator (18 kW), a capillary collimating system, and a CCD area detector. The radiation from the rotating anode with a molybdenum target is filtered by a zirconium foil so that the intensity of Kβ is 1% of that of Kα. The beam of initial size 1 mm by 0.5 mm is collimated to 0.1-mm diameter using the capillary system. A special collimator is used to reduce the size of the x-ray spot to 40 μm full width at half maximum. The diffracted x-rays were collected on a 512 by 512 pixels area detector. Data were acquired at fixed 2θ settings of 15, 25, and 30 and a sample-to-detector distance of 210 mm. Collection time in different points varied from 15 min to 12 hours. Settings of the detector were calibrated with three external independent standards (W, MgO, Al_2O_3) at each position of the detector. The sample disk was mounted on a 0.4-mm hole in a larger steel disk that was loaded onto the goniometer stage. We rotated the sample plate 30° from the initial position normal to the x-ray beam with a step of 1° in the ω axis during data collection. The position of the collimated x-ray beam penetrating through the hollandite grain was continuously monitored on a screen using a CCD camera.
21. J. Zhang, J. Ko, R. M. Hazen, C. T. Prewitt, *Am. Mineral.* **78**, 493 (1993).
22. C. B. Agee, J. Li, M. C. Shannon, S. Circone, *J. Geophys. Res.* **100**, 17725 (1995).

23. M.C. is supported by NSF of China grant 49825132 and Deutsche Forschungsgemeinschaft grant Go 315/15-1. This work was supported by the Programme National de Planétologie (CNRS-INSU). G. Montagnac helped in the Raman measurements, and B. Reynard and R. Hemley substantially improved our understanding of the Raman data.

15 December 1999; accepted 31 January 2000

Green, Catalytic Oxidation of Alcohols in Water

Gerd-Jan ten Brink, Isabel W. C. E. Arends, Roger A. Sheldon*

Alcohol oxidations are typically performed with stoichiometric reagents that generate heavy-metal waste and are usually run in chlorinated solvents. A water-soluble palladium(II) bathophenanthroline complex is a stable recyclable catalyst for the selective aerobic oxidation of a wide range of alcohols to aldehydes, ketones, and carboxylic acids in a biphasic water-alcohol system. The use of water as a solvent and air as the oxidant makes the reaction interesting from both an economic and environmental point of view.

Traditionally, oxidations of alcohols are performed with stoichiometric amounts of inorganic oxidants, notably chromium(VI) reagents (*1*). These oxidants are not only relatively expensive, but they also generate copious amounts of heavy-metal waste. Moreover, the reactions are often performed in environmentally undesirable solvents, typically chlorinated hydrocarbons. In a constant search for cleaner ("greener") technologies, there is a definite need for catalytic oxidations that use dioxygen (O_2) or hydrogen peroxide as the stoichiometric oxidant (*2*). These oxidants are atom efficient (*3*) and produce water as the only by-product.

Although the advantages of using oxygen in alcohol oxidation are evident, reports on this particular subject are still scarce. Most